PFC/JA-89-32

SELF-FIELD-INDUCED CHAOTICITY IN THE ELECTRON ORBITS IN A HELICAL-WIGGLER FREE ELECTRON LASER WITH AXIAL GUIDE FIELD

Chiping Chen and Ronald C. Davidson

July, 1989

Plasma Fusion Center
Massachusetts Institute of Technology
Cambridge, MA 02139

Research supported by the Department of Energy High Energy Physics Division, the Office of Naval Research, and the Naval Research Laboratory Plasma Physics Division.

SElF-FIELD-INDUCED CHAOTICITY IN THE ELECTRON ORBITS IN A HELICAL-WIGGLER FREE ELECTRON LASER WITH AXIAL GUIDE FIELD

Chiping Chen and Ronald C. Davidson
Plasma Fusion Center
Massachusetts Institute of Technology
Cambridge, Massachusetts 02139

ABSTRACT

The motion of a relativistic electron is analyzed in the field configuration consisting of a constant-amplitude helical wiggler magnetic field, a uniform axial magnetic field, and the equilibrium self-electric and self-magnetic fields produced by the nonneutral electron beam. By generating Poincaré surface-of-section maps, it is shown that the equilibrium self fields destroy the integrability of the motion, and consequently part of phase space becomes chaotic. In particular, the Group-I and Group-II orbits can be fully chaotic if the self fields are sufficiently strong. The threshold value of the self-field parameter $\epsilon = \omega_{pb}^2/4\Omega_c^2$ for the onset of beam chaoticity is determined numerically for parameter regimes corresponding to moderately high beam current (and density). It is found that the characteristic time scale for self-field-induced changes in the electron orbit is of the order of the time required for the beam to transit one wiggler period. An analysis of the first-order, self-field-induced resonances is carried out, and the resonance conditions and scaling relations for the resonance width are derived. The analytical estimates are in good qualitative agreement with the numerical simulations.

PACS numbers: 42.55.t, 05.45, 52.25.w

INTRODUCTION

The free electron laser (FEL)[1-3] makes use of the unstable interaction of a relativistic electron beam with a transverse wiggler magnetic field to generate coherent electromagnetic radiation.[4-8] In recent experiments,[9-13] megawatts to gigawatts of coherent radiation have been generated in the submillimeter to millimeter wavelength range. In addition, theoretical and experimental investigations[4,6,14-17] have shown that free electron lasers have several remarkable properties, including frequency tunability, high efficiency, high power, and optical guiding by the electron beam. Several FEL experiments[10-13] operate at moderately high beam current and make use of a magnetic guide field $B_0\vec{e}_z$ to steer the electron beam in the axial direction. The helical wiggler magnetic field $\vec{B}_w(\vec{x}) = -B_w(\vec{e}_x \cos k_w z + \vec{e}_y \sin k_w z)$ and the axial guide field $B_0\vec{e}_z$ then act in combination to affect the particle motion and determine the detailed properties of the free electron laser interaction.[18-22] (Here, $B_w = const.$ and $\lambda_w = 2\pi/k_w = const.$ are the wiggler amplitude and wavelength, respectively.) This paper examines the electron orbits in a helical-wiggler free electron laser with axial guide field including the effects of the equilibrium electric and magnetic self fields[23] produced by the beam space charge and current.

Although there is a considerable literature on the theory of free electron lasers, all treatments heretofore have neglected the influence of the equilibrium self fields[23] of the (nonneutral) electron beam. While such an approximation is valid for low-current FEL operation, the present analysis shows that equilibrium self-field effects play a significant role in altering the electron dynamics when the beam current I_b approaches the multi-kiloampere range. As an example, for beam radius $r_b = 0.31$cm, axial guide field $B_0 = 14.2$kG, wiggler amplitude $B_w = 710$G, wiggler wavelength $\lambda_w = 2\pi/k_w = 3.0$cm, and relativistic mass factor $\gamma_b = 3.0$, it is shown in Sec. IV that the inclusion of equilibrium self-field effects causes fully developed chaoticity in the electron orbits whenever the

beam current I_b exceeds the threshold beam current $I_b^{th} = 4.3\text{kA}$. This behavior is very different from the case where the self-electric and self-magnetic fields of the electron beam are (arbitrarily) neglected. If the equilibrium self fields are neglected, then the motion of an electron in the combined helical wiggler and axial magnetic fields is integrable and has been extensively analyzed in the literature.[18–22] In this approximation, self-consistent Vlasov-Maxwell equilibria[21] can be constructed using the single-particle constants of the motion to analyze FEL stability properties for various equilibrium profiles.[20]

A Hamiltonian system with N degrees of freedom is integrable if it has N independent constants of motion in involution, i.e., the Poisson bracket of any pair of them vanishes. If the number of constants is less than N, then the motion is nonintegrable and part of phase space is chaotic in the sense that adjacent initial conditions lead to exponentially divergent trajectories. Typically, however, there are also regular regions in phase space, consisting of the Kolmogorov-Arnold-Moser (KAM) surfaces that limit the chaotic regions of phase space.[24,25] The breakup of the KAM surfaces results in chaotic transport from one region to another, and thus the chaoticity spreads. The Poincaré surface-of-section method is useful in analyzing nonintegrable systems because the dimensionality of the Poincaré surface is $M-1$ if the motion occurs in an M-dimensional phase space.

In this paper, we analyze the motion of a relativistic electron in the field configuration consisting of a constant-amplitude helical wiggler magnetic field $\vec{B}_w(\vec{x})$, a uniform axial magnetic field $B_0\vec{e}_z$, and the equilibrium self-electric and self-magnetic fields produced by a uniform-density nonneutral electron beam with radius r_b, density n_b, and average axial velocity $V_b = const.$ It is shown that the motion is nonintegrable, possessing only two independent constants of the motion. Poincaré surface-of-section plots are generated to demonstrate the nonintegrability and chaoticity of the motion. As the dimensionless equilibrium self-field parameter $\epsilon = \omega_{pb}^2/4\Omega_c^2$ increases in size, the chaotic regions in phase space become increasingly large, leading to chaoticity. (Here, $\omega_{pb} = (4\pi n_b e^2/m)^{1/2}$ and

$\Omega_c = eB_0/mc$ are the nonrelativistic plasma and cyclotron frequencies, respectively.) The threshold value of the self-field parameter ϵ for the onset of chaoticity is found to be less than the maximum allowed value of ϵ required for radial confinement of the nonneutral electron beam. Indeed, for typical experimental parameters, values of ϵ in the range $0.01 - 0.04$ are sufficient to cause highly chaotic electron motion. Moreover, it is shown that the time scale for self-field-induced changes in the electron orbit is characterized by the time required for an electron to transit one wiggler period. This time scale is comparable with the period of oscillation about an integrable, stable, steady-state orbit calculated for $\epsilon = 0$. The first-order, self-field-induced resonances are investigated analytically, and the resonance conditions and scaling relations for the resonance width are derived.

The organization of this paper is as follows. In Sec. II, the dynamical problem is formulated in canonical variables,[26] and the constants of the motion are determined by means of canonical transformations. In Sec. III, the (integrable) motion of an electron in the wiggler and guide fields is analyzed for the case where the equilibrium self fields are negligibly small ($\epsilon = 0$). Interpretations of the canonical variables are given, and the frequencies of oscillation about the Group-I and Group-II steady-state orbits are calculated. In Sec. IV, by generating Poincaré surface-of-section maps, it is shown that the inclusion of equilibrium self-field effects ($\epsilon \neq 0$) destroys the integrability of the motion. The self-field-induced resonance conditions and scaling relations for the resonance width are derived. Finally, the threshold value of the self-field parameter for the onset of chaoticity is determined numerically for parameter regimes corresponding to moderately high beam current.

II. CANONICAL FORMULATION OF THE PROBLEM

Consider the motion of a relativistic electron in the field configuration consisting of a uniform axial magnetic field $B_0\vec{e}_z$, a constant-amplitude helical wiggler magnetic field $\vec{B}_w = -B_w(\vec{e}_x \cos k_w z + \vec{e}_y \sin k_w z)$, and the self-electric and self-magnetic fields produced by a relativistic nonneutral electron beam with radius r_b, average axial velocity $V_b\vec{e}_z$, and uniform density profile

$$n_b^0(r) = \begin{cases} n_b = const., & 0 \leq r < r_b, \\ 0, & r > r_b, \end{cases} \tag{1}$$

where $r = (x^2+y^2)^{1/2}$ is the radial distance from the beam center. Within the nonneutral electron beam ($0 \leq r < r_b$), it follows from the steady-state Maxwell equations that the equilibrium self-electric and self-magnetic fields, $\vec{E}_s$ and $\vec{B}_s$, can be expressed as[23]

$$\vec{E}_s = -\frac{m\omega_{pb}^2}{2e}(x\vec{e}_x + y\vec{e}_y), \tag{2}$$

and

$$\vec{B}_s = \frac{m\omega_{pb}^2\beta_b}{2e}(y\vec{e}_x - x\vec{e}_y). \tag{3}$$

Here, $\beta_b = V_b/c$ is the normalized beam velocity, -e and m are the electron charge and rest mass, respectively, c is the speed of light in *vacuo*, and $\omega_{pb} = (4\pi e^2 n_b/m)^{1/2}$ is the nonrelativistic plasma frequency of the beam electrons. The equations of motion for an electron within the beam ($0 \leq r < r_b$) can be derived from the Hamiltonian

$$H = \left[(c\vec{P} + e\vec{A})^2 + m^2c^4\right]^{\frac{1}{2}} - e\Phi_s \equiv \gamma mc^2 - e\Phi_s, \tag{4}$$

where $\gamma = [1 + (\vec{p}/mc)^2]^{1/2}$ is the relativistic mass factor, and the scalar and vector potentials, Φ_s and $\vec{A}$, are defined by

$$\Phi_s = \frac{m\omega_{pb}^2}{4e}(x^2 + y^2), \tag{5}$$

and

$$\vec{A} = B_0 x \vec{e}_y + A_w(\vec{e}_x \cos k_w z + \vec{e}_y \sin k_w z) + \beta_b \Phi_s \vec{e}_z, \tag{6}$$

with $A_w = B_w/k_w = const.$ The mechanical momentum $\vec{p}$ is related to the canonical momentum $\vec{P}$ by $\vec{p} = \vec{P} + e\vec{A}/c$. Because H is independent of time, the Hamiltonian is a constant of the motion, i.e.,

$$H(x, y, z, P_x, P_y, P_z) = \gamma mc^2 - e\Phi_s = const, \tag{7}$$

corresponding to the conservation of the total energy of an individual electron.

In order to find an additional constant of the motion and determine the resonances we have performed a number of canonical transformations (see Appendix A).[26] The resulting transformation to the new variables $(\varphi, \psi, z', P_\varphi, P_\psi, P_{z'})$ is given by

$$x = \left(\frac{2P_\varphi}{m\Omega_c}\right)^{\frac{1}{2}} \sin(\varphi + k_w z') - \left(\frac{2P_\psi}{m\Omega_c}\right)^{\frac{1}{2}} \cos(\psi - k_w z'), \tag{8}$$

$$y = \left(\frac{2P_\psi}{m\Omega_c}\right)^{\frac{1}{2}} \sin(\psi - k_w z') - \left(\frac{2P_\varphi}{m\Omega_c}\right)^{\frac{1}{2}} \cos(\varphi + k_w z'), \tag{9}$$

$$z = z', \tag{10}$$

$$P_x = (2m\Omega_c P_\varphi)^{\frac{1}{2}} \cos(\varphi + k_w z'), \tag{11}$$

$$P_y = (2m\Omega_c P_\psi)^{\frac{1}{2}} \cos(\psi - k_w z'), \tag{12}$$

$$P_z = P_{z'} - k_w P_\varphi + k_w P_\psi, \tag{13}$$

where $\Omega_c = eB_0/mc$ is the nonrelativistic cyclotron frequency. We shall shown in Sec. III that the canonical momenta P_φ and P_ψ characterize, respectively, the gyroradius and the guiding center radius of the steady-state orbits in the absence of the self fields. The Hamiltonian in the new variables $(\varphi, \psi, z', P_\varphi, P_\psi, P_{z'})$ is given by

$$\frac{1}{mc^2} H(\varphi, \psi, P_\varphi, P_\psi, P_{z'}) = -\frac{e\Phi_s}{mc^2} +$$
$$\left[\frac{2\Omega_c P_\varphi}{mc^2} + \frac{2eA_w}{mc^2}\left(\frac{2\Omega_c P_\varphi}{mc^2}\right)^{\frac{1}{2}} \cos\varphi + \left(\frac{P_{z'} - k_w P_\varphi + k_w P_\psi}{mc} + \beta_b \frac{e\Phi_s}{mc^2}\right)^2 + \left(\frac{eA_w}{mc^2}\right)^2 + 1\right]^{\frac{1}{2}}, \tag{14}$$

where Φ_s and ϵ are defined by

$$e\Phi_s = 2\epsilon\Omega_c[P_\varphi + P_\psi - 2(P_\varphi P_\psi)^{\frac{1}{2}} \sin(\varphi + \psi)], \tag{15}$$

$$\epsilon = \frac{\omega_{pb}^2}{4\Omega_c^2}. \tag{16}$$

The dimensionless parameter ϵ characterizes the strength of the equilibrium self fields relative to the focusing force produced by the axial guide field $B_0\vec{e}_z$.

We introduce the dimensionless parameters and variables defined by

$$\hat{\Omega}_c = \Omega_c/ck_w,\ \hat{\omega}_{pb} = \omega_{pb}/ck_w,\ \hat{\Phi}_s = e\Phi_s/mc^2,\ a_w = eA_w/mc^2,$$

$$\hat{P}_z = P_z/mc,\ \hat{P}_\varphi = k_w P_\varphi/mc,\ \hat{P}_\psi = k_w P_\psi/mc,\ \hat{H} = H/mc^2, \tag{17}$$

$$\tau = ck_w t,\ \hat{z}' = k_w z'.$$

Therefore, the Hamiltonian defined in Eq. (14) can be expressed in the dimensionless form

$$\hat{H}(\varphi, \psi, \hat{P}_\varphi, \hat{P}_\psi, \hat{P}_{z'}) =$$

$$\left[2\hat{\Omega}_c\hat{P}_\varphi + 2a_w(2\hat{\Omega}_c\hat{P}_\varphi)^{\frac{1}{2}}\cos\varphi + (\hat{P}_{z'} - \hat{P}_\varphi + \hat{P}_\psi + \beta_b\hat{\Phi}_s)^2 + a_w^2 + 1\right]^{\frac{1}{2}} - \hat{\Phi}_s, \tag{18}$$

where

$$\hat{\Phi}_s(\varphi, \psi, \hat{P}_\varphi, \hat{P}_\psi) = 2\epsilon\hat{\Omega}_c[\hat{P}_\varphi + \hat{P}_\psi - 2(\hat{P}_\varphi\hat{P}_\psi)^{\frac{1}{2}}\sin(\varphi + \psi)]. \tag{19}$$

Because $\hat{H}$ is independent of $\hat{z}'$, it follows that $\hat{P}_{z'} = const.$

In the $\epsilon = 0$ limit, where equilibrium self fields are neglected, it follows that $\hat{\Phi}_s = 0$ in Eq. (18) and the motion is integrable because $\hat{P}_\psi$ is a third constant of the motion. This limit has been analyzed extensively in the literature[18–22] and provides the traditional starting point in the formulation of FEL stability theories with an axial guide field $B_0\vec{e}_z$.[20] When $\epsilon \neq 0$, however, we shall show in Sec. IV that the motion becomes nonintegrable, with only two independent constants of the motion, $\hat{H}$ and $\hat{P}_{z'}$. As the self fields increase in intensity, the chaotic regions in phase space grow, thereby raising the question of how the self fields alter the stability properties of the FEL interaction.

It should be pointed out that the present analysis is restricted to the class of FELs with nonzero axial guide field $B_0\vec{e}_z$. [The canonical transformation in Eqs. (8)-(13) becomes singular as $B_0 \to 0$.] The effects of equilibrium self fields on the particle orbits in FEL configurations without an axial guide field are also under investigation, and the results will be the subject of a subsequent paper.

III. INTEGRABLE LIMIT

In the $\epsilon = 0$ limit, the self-field contribution vanishes ($\hat{\Phi}_s = 0$), and the Hamiltonian in Eq. (18) reduces to

$$\hat{H}_0(\varphi, \hat{P}_\varphi, \hat{P}_\psi, \hat{P}_{z'}) =$$
$$\left[2\hat{\Omega}_c\hat{P}_\varphi + 2a_w(2\hat{\Omega}_c\hat{P}_\varphi)^{\frac{1}{2}}\cos\varphi + (\hat{P}_{z'} - \hat{P}_\varphi + \hat{P}_\psi)^2 + a_w^2 + 1\right]^{\frac{1}{2}} \equiv \gamma_0, \tag{20}$$

which possesses the constants of the motion $\hat{P}_\psi$, $\hat{P}_{z'}$ and γ_0. The motion described by Eq. (20) is integrable and has been analyzed by several authors.[18–22]

The fixed points, or steady-state orbits, denoted by φ_0 and $\hat{P}_{\varphi 0}$, satisfy the steady-state equations of motion

$$\frac{d\varphi}{d\tau} = \frac{\partial\hat{H}_0}{\partial\hat{P}_\varphi} = \frac{\hat{\Omega}_c}{\gamma_0}\left[1 + \frac{a_w}{(2\hat{\Omega}_c\hat{P}_\varphi)^{\frac{1}{2}}}\cos\varphi\right] - \frac{\hat{p}_z}{\gamma_0} = 0, \tag{21}$$

$$\frac{d\hat{P}_\varphi}{d\tau} = -\frac{\partial\hat{H}_0}{\partial\varphi} = \frac{a_w}{\gamma_0}(2\hat{\Omega}_c\hat{P}_\varphi)^{\frac{1}{2}}\sin\varphi = 0, \tag{22}$$

which yield the solutions $\cos\varphi_0 = \pm 1$, and

$$(2\hat{\Omega}_c\hat{P}_{\varphi 0})^{\frac{1}{2}} = \pm\frac{a_w\hat{\Omega}_c}{\hat{p}_{z0} - \hat{\Omega}_c} > 0. \tag{23}$$

Here, $\hat{p}_{z0} = \hat{P}_{z'} - \hat{P}_{\varphi 0} + \hat{P}_\psi$ is the normalized axial mechanical momentum for $\epsilon = 0$. To locate the fixed points for given electron energy γ_0, the quantity $\hat{p}_{z0}$ is determined from the equation

$$\hat{p}_{z0}^2\left[1 + \frac{a_w^2}{(\hat{p}_{z0} - \hat{\Omega}_c)^2}\right] + 1 = \gamma_0^2, \tag{24}$$

where use has been made of Eqs. (20) and (23). Equation (24) has at most four real roots for $\hat{p}_{z0}$. For sufficiently small but nonzero $\hat{\Omega}_c$, there are three fixed points with $\hat{p}_{z0} > 0$. Among the solutions, the orbit that is stable for all $\hat{\Omega}_c > 0$ is referred to as the Group-II orbit. The other pair of stable and unstable orbits merge at $\hat{\Omega}_c = \hat{\Omega}_c^{cr}$, where the stable orbit is referred to as the stable Group-I orbit. [The normalized critical cyclotron frequency $\hat{\Omega}_c^{cr}$ is a function of a_w and γ_0 and can be determined either analytically or numerically, because Eq. (24) is fourth order in $\hat{p}_{z0}$.] Figure 1 shows the typical magnetic field dependence of $\hat{p}_{z0}$ for the integrable steady-state orbits, where the dotted straight line represents magnetoresonance ($\hat{p}_z \cong \hat{\Omega}_c$). The phase-space structure is plotted in Fig. 2 for the two cases $0 < \hat{\Omega}_c < \hat{\Omega}_c^{cr}$ and $\hat{\Omega}_c > \hat{\Omega}_c^{cr}$, where the elliptic (hyperbolic) fixed points correspond to the stable (unstable) steady-state orbits. In FEL operation, an electron beam is injected into the Group-I or Group-II orbit whenever $0 < \hat{\Omega}_c < \hat{\Omega}_c^{cr}$ or $\hat{\Omega}_c > \hat{\Omega}_c^{cr}$. Also, a cold beam with narrow energy spread is desirable to achieve high gain.

The canonical momenta P_φ and P_ψ can be interpreted as follows. From Eqs. (20) and (23), it readily follows that the phase-space trajectories for the steady-state orbits are described by $\varphi = \varphi_0$, $\psi = \psi_0 + (\hat{p}_{z0}/\gamma_0)\tau = \psi_0 + \beta_{z0}\tau$, $\hat{z}' = \hat{z}'_0 + (\hat{p}_{z0}/\gamma_0)\tau = \hat{z}'_0 + \beta_{z0}\tau$, $\hat{P}_\varphi = \hat{P}_{\varphi 0}$, $\hat{P}_\psi = \hat{P}_{\psi 0}$ and $\hat{P}_{z'} = \hat{P}_{z'0}$, where ψ_0, $\hat{z}'_0$, $\hat{P}_{\psi 0}$ and $\hat{P}_{z'0}$ are the initial conditions. Substituting this solution into Eqs. (8)-(10), the steady-state trajectories can be expressed in dimensional variables as

$$x(t) = \pm\left(\frac{2P_{\varphi 0}}{m\Omega_c}\right)^{\frac{1}{2}} \sin(k_w z_0 + k_w v_{z0} t) - \left(\frac{2P_{\psi 0}}{m\Omega_c}\right)^{\frac{1}{2}} \cos\psi_0, \tag{25}$$

$$y(t) = \mp\left(\frac{2P_{\varphi 0}}{m\Omega_c}\right)^{\frac{1}{2}} \cos(k_w z_0 + k_w v_{z0} t) + \left(\frac{2P_{\psi 0}}{m\Omega_c}\right)^{\frac{1}{2}} \sin\psi_0, \tag{26}$$

$$z = z_0 + v_{z0}t, \tag{27}$$

for $\cos\varphi_0 = \pm 1$. Equations (23)-(25) describe helical trajectories with gyroradius $r_c = (2P_{\varphi 0}/m\Omega_c)^{1/2}$ and guiding center radius $r_g = (2P_{\psi_0}/m\Omega_c)^{1/2}$, as illustrated schematically in Fig. 3. Note from Eq. (23) and the expression $r_c = (2P_{\varphi 0}/m\Omega_c)^{1/2} \propto |\hat{p}_{z0} - \hat{\Omega}_c|^{-1}$ that the effective gyroradius r_c becomes large as $\hat{p}_{z0}$ approaches $\hat{\Omega}_c$. Of course, exact magnetoresonance ($\hat{p}_z = \hat{\Omega}_c$) is avoided in FEL operation with an axial guide field $B_0\vec{e}_z$ in order to assure beam propagation and moderately small radial excursions of the transverse orbits.

It is of interest to examine the oscillatory motion near the stable orbits, expressing $\varphi = \varphi_0 + \delta\varphi$ and $\hat{P}_\varphi = \hat{P}_{\varphi 0} + \delta\hat{P}_\varphi$. It is straightforward to show, for $|\delta\varphi| << 1$ and $|\delta\hat{P}_\varphi| << \hat{P}_{\varphi 0}$, that the normalized oscillation frequencies for both Group-I and Group-II orbits are given by

$$\hat{\omega} = \frac{|\hat{p}_{z0} - \hat{\Omega}_c|}{\gamma_0}\left[1 - \frac{\hat{\Omega}_c}{a_w}\left(\frac{\hat{p}_{t0}}{\hat{p}_{z0}}\right)^3\right]^{\frac{1}{2}}. \tag{28}$$

Here, the normalized transverse mechanical momentum $\hat{p}_{t0}\vec{e}_1$ is given by

$$\hat{p}_{t0}\vec{e}_1 = \frac{a_w\hat{p}_{z0}}{\hat{p}_{z0} - \hat{\Omega}_c}\vec{e}_1, \tag{29}$$

where $\vec{e}_1 = \vec{e}_x \cos k_w z + \vec{e}_y \sin k_w z$. For $|\hat{p}_{t0}/\hat{p}_z|^3 << a_w/\hat{\Omega}_c$, it follows from Eq. (28) that $\hat{\omega} \cong |\hat{p}_z - \hat{\Omega}_c|/\gamma_0$, thereby recovering the results in Refs. 18 and 20.

IV. CHAOTIC MOTION

In this section, it is shown that the equilibrium self-field contribution Φ_s in Eq. (18) destroys the integrability of the motion. In particular, the stable steady-state orbits calculated in Sec. III become chaotic if the self fields are sufficiently strong. The equations of motion for $\epsilon \neq 0$ are obtained from the Hamiltonian defined in Eq. (18). This gives

$$\frac{d\hat{\varphi}}{d\tau} = \frac{\partial \hat{H}}{\partial \hat{P}_\varphi} = -\frac{\hat{p}_z}{\gamma} + \frac{\hat{\Omega}_c}{\gamma}\Big[1 + \frac{a_w}{(2\hat{\Omega}_c \hat{P}_\varphi)^{\frac{1}{2}}}\cos\varphi\Big] - 2\epsilon\hat{\Omega}_c\Big(1 - \beta_b\frac{\hat{p}_z}{\gamma}\Big)\Big[1 - \Big(\frac{\hat{P}_\psi}{\hat{P}_\varphi}\Big)^{\frac{1}{2}}\sin(\varphi+\psi)\Big], \tag{30}$$

$$\frac{d\hat{\psi}}{d\tau} = \frac{\partial \hat{H}}{\partial \hat{P}_\psi} = \frac{\hat{p}_z}{\gamma} - 2\epsilon\hat{\Omega}_c\Big(1 - \beta_b\frac{\hat{p}_z}{\gamma}\Big)\Big[1 - \Big(\frac{\hat{P}_\varphi}{\hat{P}_\psi}\Big)^{\frac{1}{2}}\sin(\varphi+\psi)\Big], \tag{31}$$

$$\frac{d\hat{P}_\varphi}{d\tau} = -\frac{\partial \hat{H}}{\partial \varphi} = \frac{a_w}{\gamma}(2\Omega_c\hat{P}_\varphi)^{\frac{1}{2}}\cos\varphi - 4\epsilon\hat{\Omega}_c\Big(1 - \beta_b\frac{\hat{p}_z}{\gamma}\Big)(\hat{P}_\varphi\hat{P}_\psi)^{\frac{1}{2}}\cos(\varphi+\psi), \tag{32}$$

$$\frac{d\hat{P}_\psi}{d\tau} = -\frac{\partial \hat{H}}{\partial \psi} = -4\epsilon\hat{\Omega}_c\Big(1 - \beta_b\frac{\hat{p}_z}{\gamma}\Big)(\hat{P}_\varphi\hat{P}_\psi)^{\frac{1}{2}}\cos(\varphi+\psi), \tag{33}$$

where the normalized axial mechanical momentum $\hat{p}_z = \hat{P}_{z'} - \hat{P}_\varphi + \hat{P}_\psi + \beta_b\hat{\Phi}_s(\varphi, \psi, \hat{P}_\varphi, \hat{P}_\psi)$ has been introduced for simplicity of notation. Note that the constancy of γ_0 in Sec. III is now replaced by $\hat{H} = \gamma - \hat{\Phi}_s$, where $\hat{P}_\psi$ is no longer a constant of the motion.

It is important to compare the characteristic time scale T_s for the self-field-induced changes in the particle orbit with the period of oscillation T_0 about the stable Group-I or Group-II orbit calculated in Eq. (28). Here, $T_0 = 2\pi/ck_w\hat{\omega} = \lambda_w/c\hat{\omega}$, where $\hat{\omega}$ is of order unity and $\lambda_w = 2\pi/k_w$ is the wiggler period. The time scale T_s can be estimated from the rate of change of the phase in $\hat{\Phi}_s$ in Eq. (19) for the integrable stable steady-state orbit, i.e., from $\dot{\varphi} + \dot{\psi} \cong \dot{\psi} = k_w v_z + O(\epsilon) \cong k_w V_b$, where the super-dot designates

the derivative with respect to time t. Therefore, the time scale associated with self-field effects is $T_s \approx \lambda_w/V_b$, which is the time required for a beam electron to transit one wiggler period λ_w. The fact that T_s and T_0 are comparable in size implies that the equilibrium self fields can rapidly affect the motion of the beam electron. Because the motion apparently does not possess a third constant of the motion for $\epsilon \neq 0$, chaoticity is expected to be observable and to spread significantly before the electron beam passes through multiple wiggler periods, even for modest values of ϵ. In contrast to the chaoticity induced by an electromagnetic perturbation with time scale characterized by the synchrotron period of an electron moving in the ponderomotive potential,[27] chaotic behavior arising from equilibrium self-field effects is likely to be more harmful to FEL operation. It is known that sidebands also cause chaotic behavior,[28,29] which is not likely to be important until nonlinear saturation occurs.

To provide a semi-quantitative understanding of the nonintegrable motion near the Group-I or Group-II orbit, the first-order self-field-induced resonances are analyzed as follows. For $\epsilon << 1$, the Hamiltonian in Eq. (18) can be expanded to first order in ϵ according to

$$\hat{H} \cong \hat{H}_0 + \epsilon \hat{H}_1, \tag{34}$$

where

$$\hat{H}_1 = 2\hat{\Omega}_c\left(1 - \beta_b \frac{\hat{P}_z}{\gamma_0}\right)[\hat{P}_\varphi + \hat{P}_\psi - 2(\hat{P}_\varphi \hat{P}_\psi)^{\frac{1}{2}} \sin(\phi + \psi)], \tag{35}$$

and the zero-order Hamiltonian $\hat{H}_0 = \gamma_0$ defined in Eq. (20) is integrable. For an electron oscillating about an integrable stable steady-state orbit described by $\varphi(\tau) = \varphi_0 + \delta\varphi_0 \cos\hat{\omega}\tau$ and $\hat{P}_\varphi = \hat{P}_{\varphi 0} + \delta\hat{P}_\varphi \sin\hat{\omega}\tau$, the perturbation $\hat{H}_1$ can be approximated by

$$\hat{H}_1 \cong 2\hat{\Omega}_c(1-\beta_b^2)\{\hat{P}_{\varphi 0}+\hat{P}_{\psi 0}-2(\hat{P}_{\varphi 0}\hat{P}_{\psi 0})^{\frac{1}{2}}\sin[\varphi_0+\delta\varphi_0\cos\hat{\omega}\tau+\psi]\}$$

$$=2\hat{\Omega}_c(1-\beta_b^2)\Big\{\hat{P}_{\varphi 0}+\hat{P}_{\psi 0}-2(\hat{P}_{\varphi 0}\hat{P}_{\psi 0})^{\frac{1}{2}}\sum_{n=-\infty}^{\infty}J_n(\delta\varphi_0)\sin\Big[\Big(\hat{\omega}\tau+\frac{\pi}{2}\Big)n+\psi+\varphi_0\Big]\Big\}. \quad (36)$$

Here, $\hat{\omega}$ is defined in Eq. (28), $J_n(x)$ is the Bessel function of the first kind of order n, and use has been made of the approximation $\beta_{z0}\cong\beta_b$. It follows from Eq. (36) that the self-field-induced resonances are given by

$$\frac{d\psi}{d\tau}+n\hat{\omega}=0, \qquad n=0,\pm1,\pm2,\cdots. \quad (37)$$

Substituting Eqs. (28) and (31) into Eq. (37) and averaging over the oscillation period $2\pi/\hat{\omega}$, we obtain the resonance condition

$$n\frac{|\hat{p}_{z0}-\hat{\Omega}_c|}{\gamma_0}\Big[1-\frac{\hat{\Omega}_c}{a_w}\Big(\frac{\hat{p}_{t0}}{\hat{p}_{z0}}\Big)^3\Big]^{\frac{1}{2}}+\frac{\hat{p}_{z0}}{\gamma_0}-2\epsilon\hat{\Omega}_c\Big(1-\beta_b\frac{\hat{p}_{z0}}{\gamma_0}\Big)=0. \quad (38)$$

Figure 4 shows plots of the resonance curves (the solid curves) corresponding to the solutions to Eq. (38) for $n=-1,-2$ and -3. The dashed curves in Fig. 4 are the integrable steady-state orbits calculated in Fig. 1. In Fig. 4, the intersections (marked by the dots) between the integrable stable orbits and the resonance curves labeled by the integer n correspond to rational orbits. That is, the electron rotates through an angle of $2\pi/n$ about the fixed point as ψ advances by 2π. It readily follows from Eqs. (20), (34) and (36) that the normalized resonance width $\hat{w}_n$ of $\hat{p}_z$ can be estimated by

$$\hat{w}_n=[32\epsilon\gamma_b\hat{\Omega}_c|J_n(\delta\varphi_0)|]^{\frac{1}{2}}(\hat{P}_{\varphi 0}\hat{P}_{\psi 0})^{\frac{1}{4}}, \quad (39)$$

or equivalently,

$$\hat{w}_n=4\Big[\frac{\gamma_b r_c r_g I_b|J_n(\delta\varphi_0)|}{\beta_b r_b^2 I_A}\Big]^{\frac{1}{2}}. \quad (40)$$

Here, r_b, I_b and $\gamma_b mc^2$ are the radius, current and energy of the electron beam, $I_A = mc^3/e \cong 17\text{kA}$ is the Alfvén current, and r_c and r_g are the gyroradius and the guiding center radius, respectively, as illustrated in Fig. 3. Use has been made of the relation $\epsilon = \omega_{pb}^2/4\Omega_c^2 = (c^2/\Omega_c^2 r_b^2 \beta_b)(I_b/I_A)$ in deriving Eq. (40) from Eq. (39). The scaling relations in Eqs. (39) and (40) exhibit a strong dependence of $\hat{\omega}_n$ on equilibrium self-field effects. In particular, $\hat{\omega}_n$ is directly proportional to $(I_b/I_A)^{1/2}$. Note also that $\hat{\omega}_n$ is proportional to $(r_g/r_b)^{1/2}$, so that the resonance width is largest for electrons with guiding center radius r_g approaching the beam radius r_b. In addition, the factor $r_c^{1/2}$ in Eq. (40) is proportional to $|\hat{p}_{z0} - \hat{\Omega}_c|^{-1}$, which becomes increasingly large near magnetoresonance.

Poincaré surface-of-section maps have been generated by numerically integrating the equations of motion in Eqs. (30)-(33). This analysis demonstrates the chaotic motion and illustrates that the earlier analytical estimates have captured the underlying physics involved in the nonlinear dynamics of an individual electron. The motion described by Eqs. (30)-(33) occurs in the three-dimensional phase space $(\varphi, \psi, \hat{P}_\psi)$, because $\hat{P}_\varphi$ is determined from the constancy of $\hat{H}$ and $\hat{P}_{z'}$. In order to compare with the integrable phase plane in Fig. 2, the plane $(\varphi, \hat{p}_z)$ with $\psi = 0$, mod 2π, is chosen to be the surface-of-section in the numerical calculations. It follows from Eq. (33) that the variation of $\hat{P}_\psi$ is small for small ϵ. The effective normalized guiding center radius $\hat{r}_g \cong (2\hat{P}_\psi/\hat{\Omega}_c)^{1/2}$ is specified by the initial condition for $\hat{P}_\psi$. It should be pointed out that on a surface of constant energy, with fixed initial conditions for φ, ψ and $\hat{P}_\psi$, different initial conditions for the axial mechanical momentum $\hat{p}_z$ are accomplished by choosing different values for the axial canonical momentum $\hat{P}_{z'}$ and different initial conditions for $\hat{P}_\varphi$.

Figure 5 shows typical nonintegrable surface-of-section plots for the two cases: (a) $0 < \hat{\Omega}_c < \hat{\Omega}_c^{cr}$, and (b) $\hat{\Omega}_c > \hat{\Omega}_c^{cr}$. The values of the dimensionless parameters in Fig. 5 are: (a) $\epsilon = 0.01$, $\hat{\Omega}_c = 2.0$, $\hat{H} = 3.0$, $a_w = 0.2$ and $\beta_b = 0.91$, and (b) $\epsilon = 0.01$, $\hat{\Omega}_c = 4.0$, $\hat{H} = 3.0$, $a_w = 0.2$ and $\beta_b = 0.93$. In obtaining the results in Fig. 5, the beam radius r_b

is assumed to be sufficiently large that the maximum radial excursion of an individual electron remains within the electron beam, where the self fields are described by Eqs. (2) and (3). In addition, the initial condition for $\hat{P}_\psi$ is fixed at the value $(2\hat{P}_{\psi 0}/\hat{\Omega}_c)^{1/2} = 0.25$, whereas the initial condition for $\hat{p}_z$ is allowed to vary in Fig. 5. By comparing Fig. 5(a) with Fig. 2(a), although there is little change in the vicinity of the Group-I orbit, it is evident that the Group-II orbit is chaotic as a result of equilibrium self-field effects. This agrees qualitatively with the scaling relations in Eqs. (39) and (40) because the Group-I orbit is further removed from magnetoresonance than the Group-II orbit. In Fig. 5(b), a period-two island appears near the Group-II orbit. This is also in agreement with the earlier resonance analysis because the Group-II orbit nearly intersects the resonance curve with $n = -2$ at $\hat{\Omega}_c = 4.0$ in Fig. 4. Although the nonintegrability and chaoticity of the motion are evident in Fig. 5, the Group-I orbit in Fig. 5(a) and the Group-II orbit in Fig. 5(b) remain almost regular. That is, the equilibrium self fields ($\epsilon = 0.01$) in Fig. 5 are not sufficiently strong to cause significant chaoticity in the particle orbits.

The onset of chaoticity of the Group-II orbit is shown in the surface-of-section plot in Fig. 6 for $\epsilon = 0.04$, $\hat{\Omega}_c = 4.0$, $\hat{H} = 3.0$, $a_w = 0.2$, $\beta_b = 0.93$ and $k_w r_b = 0.65$. In Fig. 6, the normalized effective gyroradius $(2\hat{P}_\phi/\Omega_c)^{1/2}$ ranges from 0.17 to 0.35, and the normalized guiding center radius is $(2\hat{P}_\psi/\hat{\Omega}_c)^{1/2} \cong 0.25$. Note that the threshold value of the self-field parameter ($\epsilon = 0.04$) for the onset of chaoticity is much less than the limiting value of the self-field parameter $\{\epsilon = [8\gamma_b(1-\beta_b^2)]^{-1} = 0.3\}$ for radial confinement of the beam electrons.[23] As an example, for $\lambda_w = 3.0$cm, the dimensionless parameters in Fig. 6 correspond to $r_b = 0.31$cm, $I_b = 4.3$kA, $B_w = 710$G, $B_0 = 14.2$kG, $\beta_b = 0.93$ and $\gamma_b = 3.0$.

V. CONCLUSIONS

In this paper we have investigated the effects of equilibrium self fields on the electron orbits in a helical-wiggler FEL with an axial guide field $B_0\vec{e}_z$. It was shown that the equilibrium self fields destroy the integrability of the motion, and consequently part of phase space becomes chaotic. In particular, the Group-I and Group-II orbits can be chaotic if the equilibrium self fields are sufficiently strong. Typically, the threshold value of the self-field parameter $\epsilon = \omega_{pb}^2/4\Omega_c^2$ for the onset of chaoticity is larger than the self-field parameters in present-day FEL experiments, which operate at moderate beam current. Furthermore, the time scale for self-field-induced changes in the electron orbit is characterized by the time required for an electron to transit one wiggler period. This results in a rapid spread of chaoticity in momentum space as the electron beam passes through a few wiggler periods. In this regard, the influence of equilibrium self fields differs significantly from the effect of an electromagnetic perturbation[27] which induces chaoticity on a (long) time scale characterized by the synchrotron period of an electron in the ponderomotive potential. Further investigations are required to understand how self-field-induced chaoticity alters the stability properties of the FEL interaction.

ACKNOWLEDGEMENTS

This work was supported by the Department of Energy High Energy Physics Division, the Office of Naval Research, and the Naval Research Laboratory Plasma Physics Division.

APPENDIX A: CANONICAL TRANSFORMATIONS

To verify that the transformation given in Eqs. (8)-(13) is indeed canonical, we first perform the canonical transformation among the transverse variables,[26]

$$x = \left(\frac{2P_\alpha}{m\Omega_c}\right)^{\frac{1}{2}} \sin\alpha - \frac{P_Y}{m\Omega_c},\ y = Y - \left(\frac{2P_\alpha}{m\Omega_c}\right)^{\frac{1}{2}} \cos\alpha,$$

$$P_x = (2m\Omega_c P_\alpha)^{\frac{1}{2}} \cos\alpha,\ P_y = P_Y, \tag{A1}$$

given by the generating function

$$F_3(P_x, P_y; \alpha, Y) = \frac{1}{m\Omega_c}(P_x P_y - \frac{P_x^2}{2}\tan\alpha) - YP_y, \tag{A2}$$

where $\Omega_c = eB_0/mc$. Substituting Eqs. (5)-(6) and (A1) into Eq. (4) yields

$$H(\alpha, Y, z, P_\alpha, P_Y, P_z) =$$

$$\left[2mc^2\Omega_c P_\alpha + 2eA_w(2mc^2\Omega_c P_\alpha)^{\frac{1}{2}}\cos(\alpha - k_w z) + (cP_z + e\beta_b\Phi_s)^2 + (eA_w)^2 + m^2c^4\right]^{\frac{1}{2}} - e\Phi_s, \tag{A3}$$

where

$$e\Phi_s = \frac{m\omega_b^2}{4}\left\{\left[\left(\frac{2P_\alpha}{m\Omega_c}\right)^{\frac{1}{2}}\sin\alpha - \frac{P_Y}{m\Omega_c}\right]^2 + \left[Y - \left(\frac{2P_\alpha}{m\Omega_c}\right)^{\frac{1}{2}}\cos\alpha\right]^2\right\}. \tag{A4}$$

Second, we introduce the polar coordinates β and P_β in the $Y - P_Y$ phase plane,

$$Y = \left(\frac{2P_\beta}{m\Omega_c}\right)^{\frac{1}{2}}\sin\beta,\ P_Y = (2m\Omega_c P_\beta)^{\frac{1}{2}}\cos\beta, \tag{A5}$$

with the generating function

$$F_1(Y;\beta) = \frac{m\Omega_c Y^2}{2}\cot\beta. \tag{A6}$$

The Hamiltonian is then transformed to

$$H(\alpha,\beta,z,P_\alpha,P_\beta,P_z) =$$

$$\left[2mc^2\Omega_c P_\alpha + 2eA_w(2mc^2\Omega_c P_\alpha)^{\frac{1}{2}}\cos(\alpha - k_w z) + (cP_z + e\beta_b\Phi_s)^2 + (eA_w)^2 + m^2c^4\right]^{\frac{1}{2}} - e\Phi_s, \tag{A7}$$

where Φ_s is defined by

$$e\Phi_s = 2\epsilon\Omega_c[P_\alpha + P_\beta - 2(P_\alpha P_\beta)^{\frac{1}{2}}\sin(\alpha+\beta)]. \tag{A8}$$

Here, ϵ is the self-field parameter defined in Eq. (16). Finally, the canonical transformation,

$$\varphi = \alpha - k_w z,\ \psi = \beta + k_w z,\ z' = z, \tag{A9}$$

$$P_\varphi = P_\alpha,\ P_\psi = P_\beta,\ P_{z'} = P_z + k_w(P_\varphi - P_\psi),$$

with the generating function

$$F_2(\alpha,\beta,z';P_\varphi,P_\psi,P_{z'}) = (\alpha - k_w z)P_\varphi + (\beta + k_w z)P_\psi + zP_{z'}, \tag{A10}$$

yields the resulting canonical transformation in Eqs. (8)-(13) and the Hamiltonian in Eq. (14).

REFERENCES

1. *Free Electron Laser Handbook*, eds., W. Colson, C. Pellegrini and A. Renieri (North-Holland, Amsterdam, 1989).
2. C.W. Roberson and P. Sprangle, Phys. Fluids B1, 3 (1989).
3. T.C. Marshall, *Free Electron Lasers* (Macmillan, New York, 1985).
4. N.M. Kroll, P.L. Morton and M.N. Rosenbluth, IEEE J. Quantum Electron. **17**, 1436 (1981).
5. R.C. Davidson and H.S. Uhm, Phys. Fluids **23**, 2076 (1980).
6. P. Sprangle, R.A. Smith and V.L. Granatstein, in *Infrared and Millimeter Waves*, ed., K.J. Button (Academic Press, New York, 1979), Volume **1**, p. 297.
7. D.B. McDermott, T.C. Marshall, S.P. Schlesinger, R.K. Parker and V.L. Granatstein, Phys. Rev. Lett. **41**, 1368 (1978).
8. D.A.G. Deacon, L.R. Ellis, J.M.J. Madey, G.J. Ramian, H.A. Schwettman and T.I. Smith, Phys. Rev. Lett. **38**, 892 (1977).
9. T. J. Orzechowski, B.R. Anderson, J.C. Clark, W.M. Fawley, A.C. Paul, D. Prosnitz, E.T. Scharlemann, S.M. Yarema, D.B. Hopkins, A.M. Sessler, J.S. Wurtele, Phys. Rev. Lett. **57**, 2172 (1986).
10. J. Masud, T.C. Marshall, S.P. Schlesinger and F.G. Yee, Phys. Rev. Lett. **56**, 1567 (1986).
11. J. Fajans, G. Bekefi, Y.Z. Yin and B. Lax, Phys. Fluids **28**, 1995 (1985).
12. S.H. Gold, W.M. Black, H.P. Freund, V.L. Granatstein, R.H. Jackson, P.C. Efthimion and A.K. Kinkead, Phys. Fluids **26**, 2683 (1983).
13. R.K. Parker, R.H. Jackson, S.H. Gold, H.P. Freund, V.L. Granatstein, P.C. Efthimion, M. Herndon and A.K. Kinkead, Phys. Rev. Lett. **48**, 238 (1982).

14. J. Fajans, J.S. Wurtele, G. Bekefi, D.S. Knowles and K. Xu, Phys. Rev. Lett. **57**, 579 (1986).

15. E.T, Scharlemann, A.M. Sessler and J.S. Wurtele, Phys. Rev. Lett. **54**, 1925 (1985).

16. P. Sprangle and C.M. Tang, Appl. Phys. Lett. **39**, 677 (1981).

17. D. Prosnitz, A. Szoke and V.K. Neil, Phys. Rev. A**24** 1936 (1981).

18. H.P. Freund and A. K. Ganguly, Phys. Rev. A**28**, 3438 (1983).

19. H.P. Freund, Phys. Rev. A**27**, 1977 (1983).

20. H.P. Freund P. Sprangle, D. Dillenburg, E.H. da Jornada, R.S. Schneider and B. Liberman, Phys. Rev. A**26**, 2004 (1982).

21. R.C. Davidson and H.S. Uhm, J. Appl. Phys. **53**, 2910 (1982).

22. L. Friedland, Phys. Fluids **23**, 2376 (1980).

23. R.C. Davidson, *Theory of Nonneutral Plasmas*, (Addison-Wesley, Reading, Massachusetts, 1989).

24. M. V. Berry, in *Topics of Nonlinear Dynamics*, ed., S. Jorna, AIP Conference Proceedings, (American Institute of Physics, New York, 1978), No. 46, p. 16.

25. A.J. Lichtenberg and M.A. Lieberman, *Regular and Stochastic Motion* (Springer-Verlag, New York, 1983).

26. H. Goldstein, *Classical Mechanics*, (Addison-Wesley, Reading, Massachusetts, 1980).

27. C. Chen and G. Schmidt, Comments in Plasma Physics and Controlled Fusion **12**, 83 (1988).

28. R.C. Davidson and J.S. Wurtele, Phys. Fluids **30**, 557 (1987).

29. S. Riyopoulos and C.M. Tang, Nucl. Instrum. Methods A**259**, 226 (1987).

FIGURE CAPTIONS

Fig. 1. Plot of the integrable steady-state orbits calculated from Eq. (24) for $\epsilon = 0$, $\gamma_0 = 3.0$ and $a_w = 0.2$. The solid (dashed) curves correspond to the stable (unstable) orbits, and the dotted straight line designates the magnetoresonance condition $\hat{p}_z = \hat{\Omega}_c$.

Fig. 2. Contour plots in the integrable phase plane (φ, p_z) calculated from Eq. (20) for $\epsilon = 0$, $\gamma_0 = 3.0$ and $a_w = 0.2$. The two cases correspond to (a) $\hat{\Omega}_c = 2.0 < \hat{\Omega}_c^{cr} \cong 2.1$, and (b) $\hat{\Omega}_c = 4.0 > \hat{\Omega}_c^{cr}$.

Fig. 3. Projections in the plane (x,y) of the integrable steady-state trajectory given in Eqs. (25)-(27) for $\cos\varphi_0 = +1$. Here, $r_g = (2P_{\psi 0}/m\Omega_c)^{\frac{1}{2}}$ and $r_c = (2P_{\varphi 0}/m\Omega_c)^{\frac{1}{2}}$ are the guiding center radius and the gyroradius, respectively.

Fig. 4. The equilibrium self-field resonance curves (solid curves) correspond to the solutions to Eq. (36) for $n = -1, -2, -3$, $\epsilon = 0.01$, $\gamma_0 = 3.0$ and $a_w = 0.2$. The dashed curves are the integrable steady-state orbits calculated in Fig. 1, and the dots signify the intersections between the resonance curves and the steady-state orbits.

Fig. 5. Typical nonintegrable surface-of-section plots with $\psi = 0$, mod 2π, for the two cases (a) $0 < \hat{\Omega}_c = 2.0 < \hat{\Omega}_c^{cr} \cong 2.1$, and (b) $\hat{\Omega}_c = 4.0 > \hat{\Omega}_c^{cr}$. Other system parameters are (a) $\epsilon = 0.01$, $\hat{H} = 3.0$, $a_w = 0.2$ and $\beta_b = 0.91$, and (b) $\epsilon = 0.01$, $\hat{H} = 3.0$, $a_w = 0.2$ and $\beta_b = 0.93$.

Fig. 6. The surface-of-section plot at the onset of chaoticity of the Group-II orbit for the choice of system parameters $\epsilon = 0.04$, $\hat{\Omega}_c = 4.0$, $\hat{H} = 3.0$, $a_w = 0.2$ and $\beta_b = 0.93$. In this plot, the normalized effective gyroradius $(2\hat{P}_\varphi/\hat{\Omega}_c)^{1/2}$ ranges

from 0.17 to 0.35, the normalized guiding center radius is $(2\hat{P}_\psi/\hat{\Omega}_c)^{1/2} \cong 0.25$, and the normalized beam radius is $k_w r_b = 0.65$.

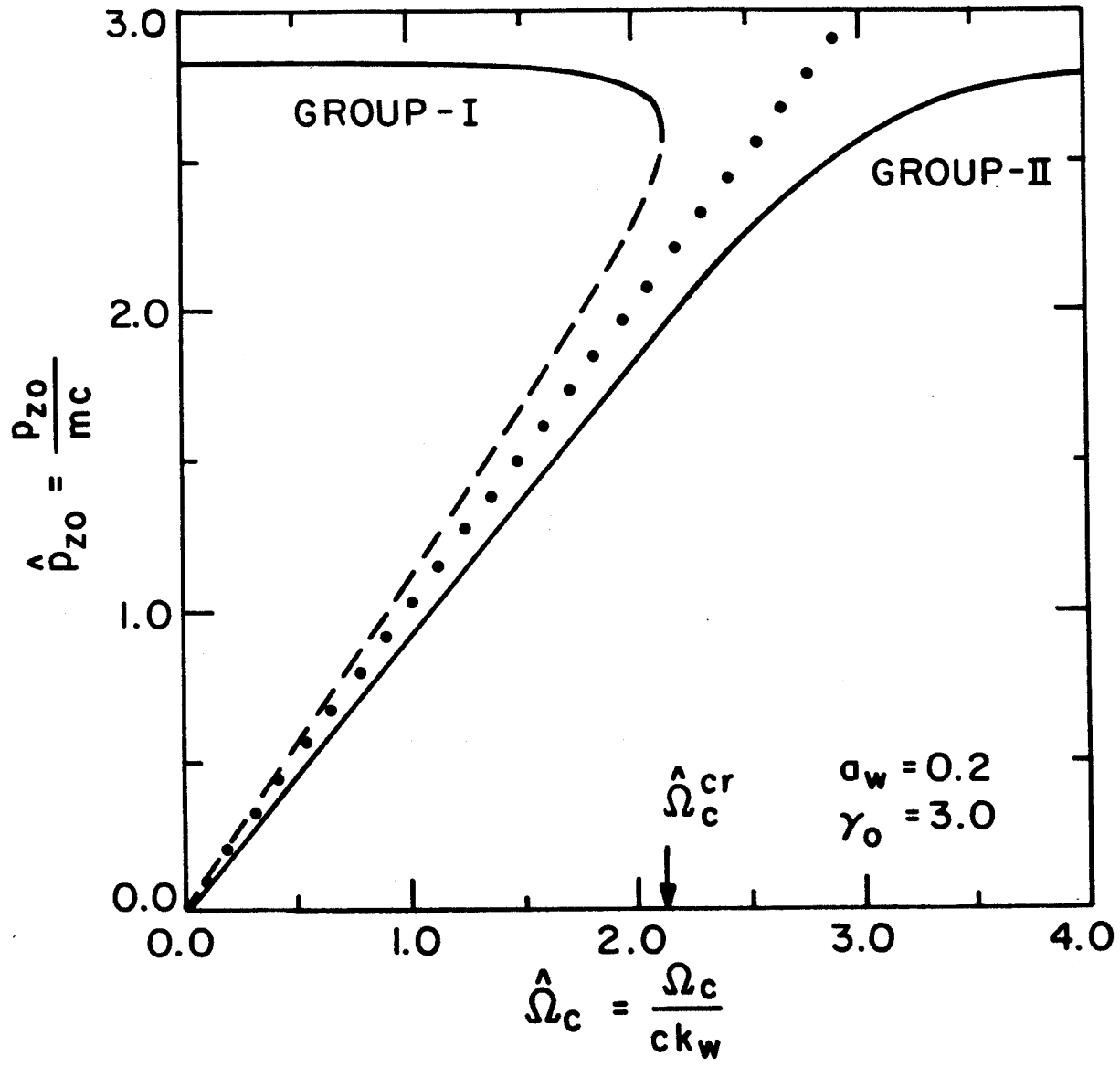
3.0
2.0
1.0
0.0
GROUP-I
GROUP-II
$\hat{p}_{zo} = \frac{p_{zo}}{mc}$
$\hat{\Omega}_c^{cr}$
$a_w = 0.2$
$\gamma_o = 3.0$
0.0
1.0
2.0
3.0
4.0
$\hat{\Omega}_c = \frac{\Omega_c}{ck_w}$

Figure 1

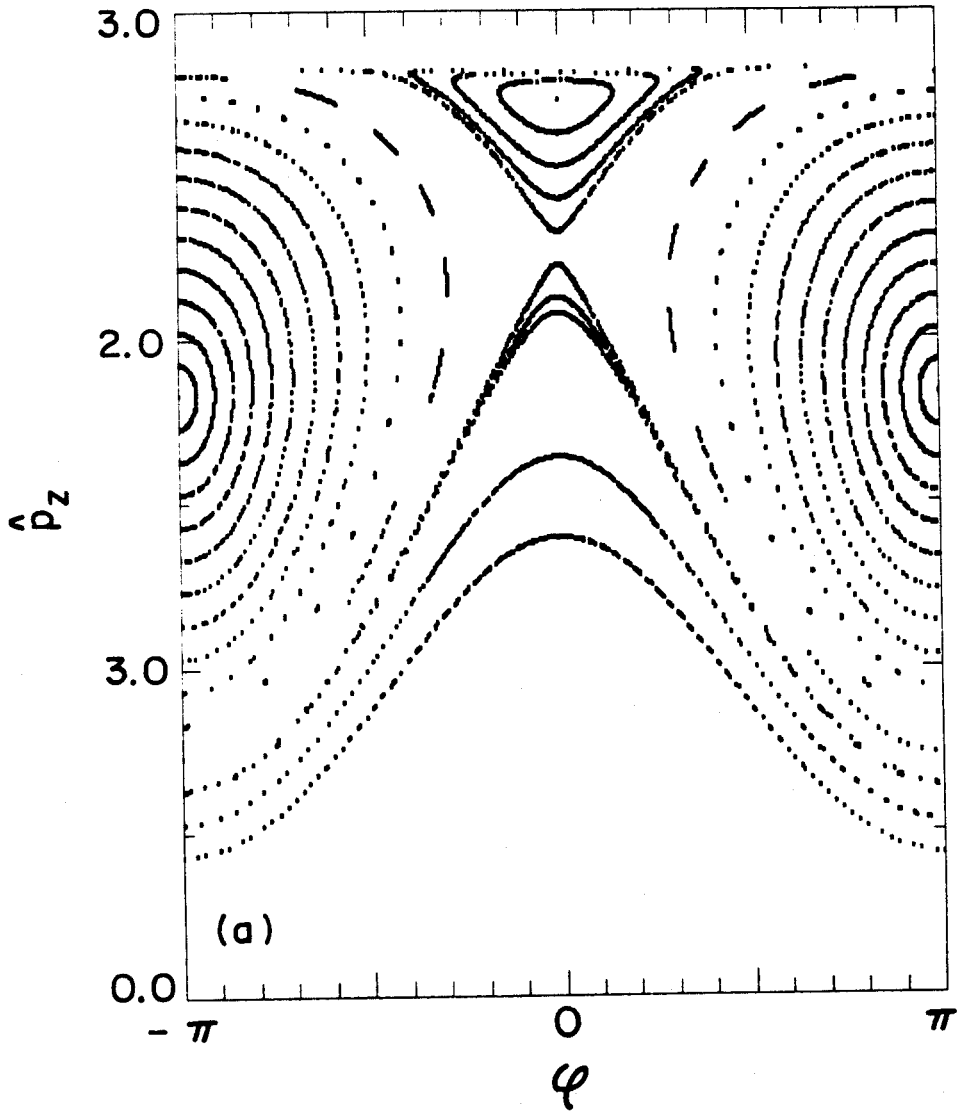

Figure 2a

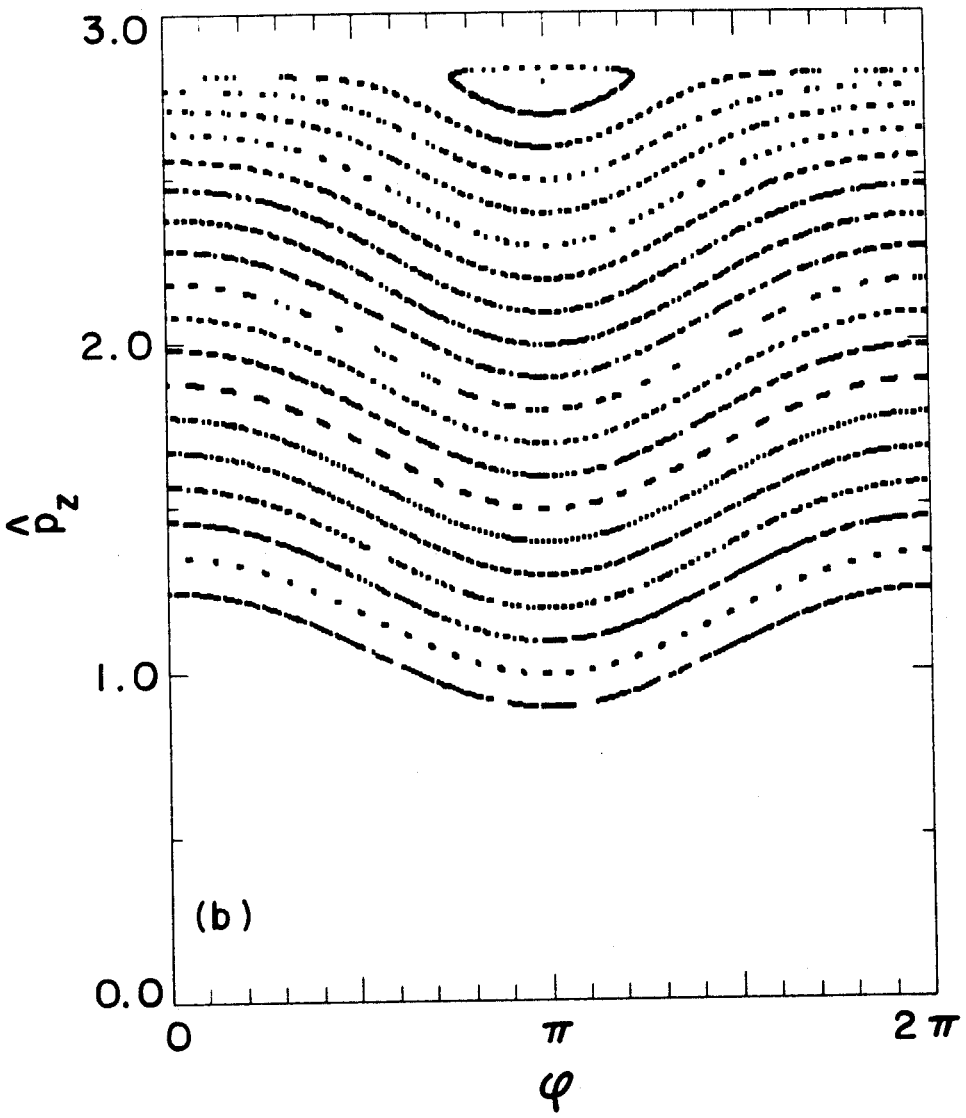

Figure 2b

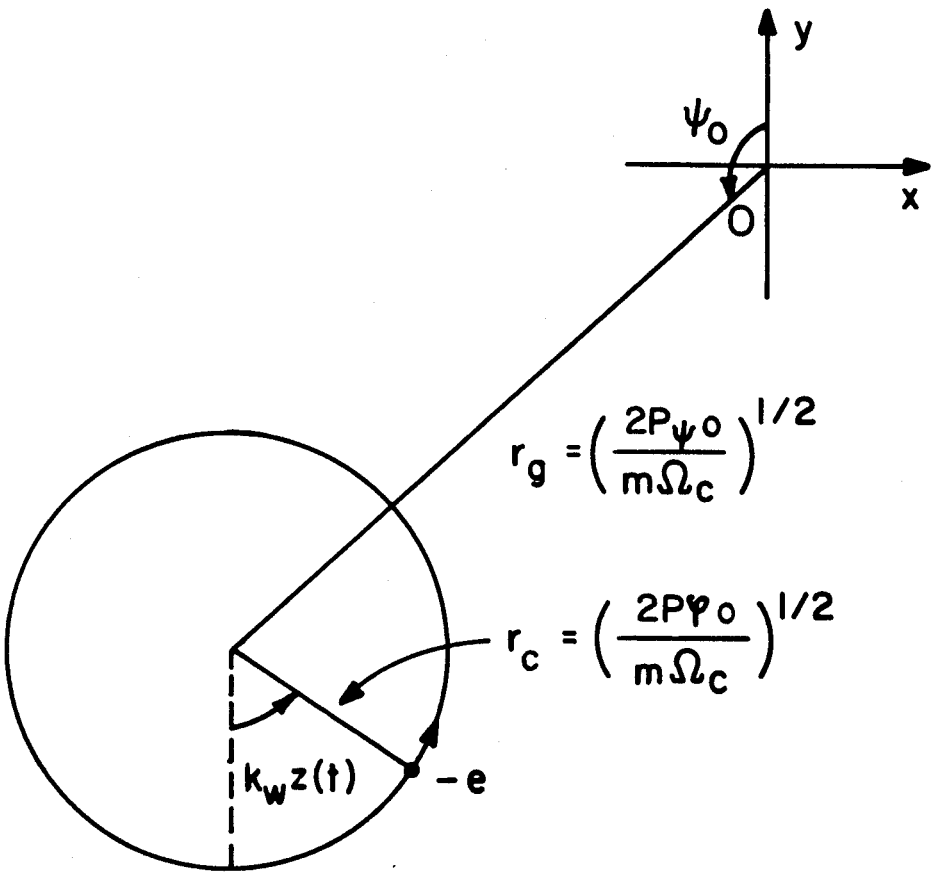
y
ψ_o
x
O
$r_g = \left(\frac{2P_{\psi o}}{m\Omega_c}\right)^{1/2}$
$r_c = \left(\frac{2P_{\psi o}}{m\Omega_c}\right)^{1/2}$
$k_w z(t)$
-e

Figure 3

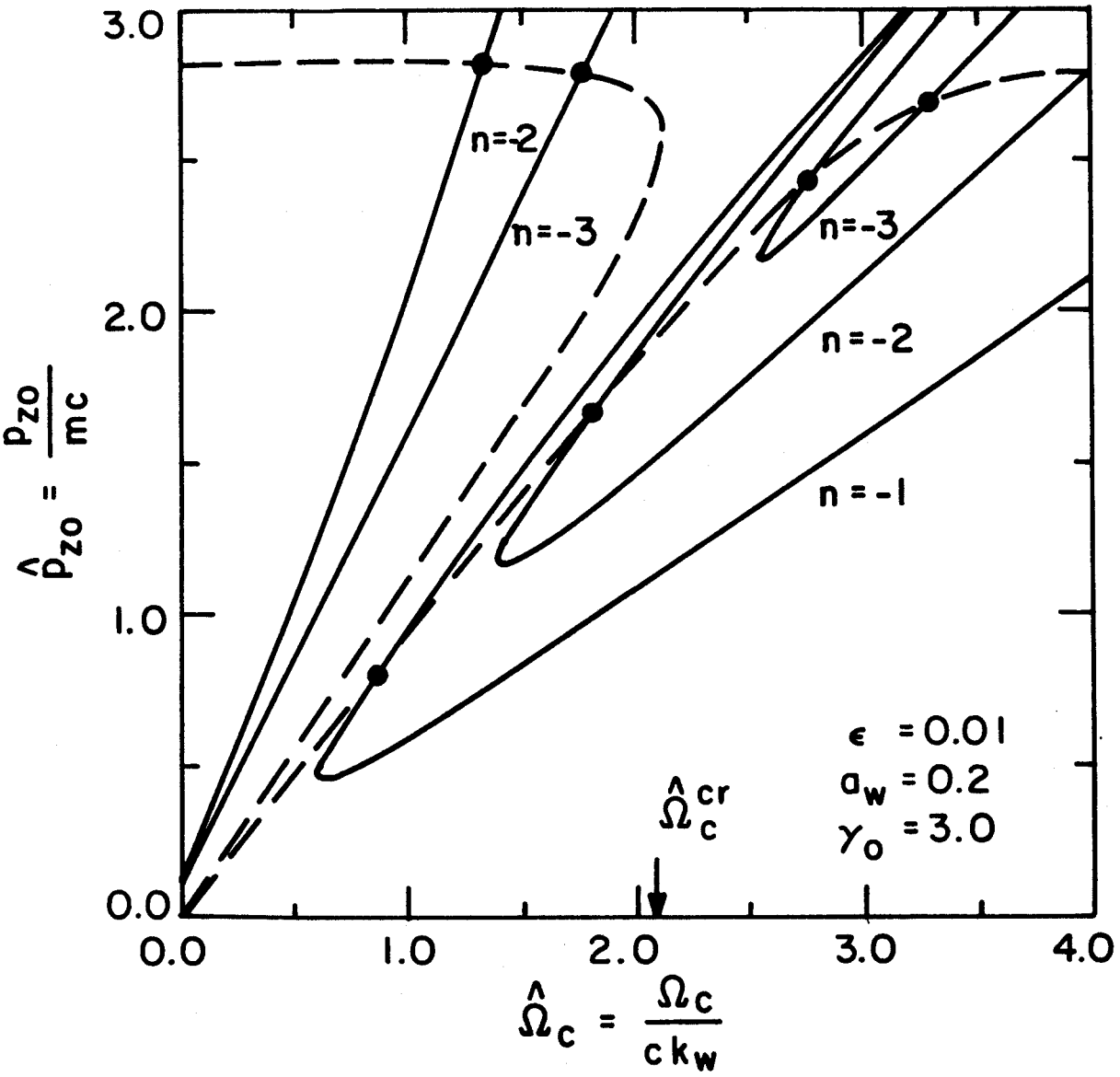
3.0
2.0
1.0
0.0
0.0
1.0
2.0
3.0
4.0
n=-2
n=-3
n=-3
n=-2
n=-1
ϵ =0.01
a_w = 0.2
γ_0 = 3.0
$\hat{\Omega}_c^{cr}$
$\hat{p}_{z0} = \frac{p_{z0}}{mc}$
$\hat{\Omega}_c = \frac{\Omega_c}{c k_w}$

Figure 4

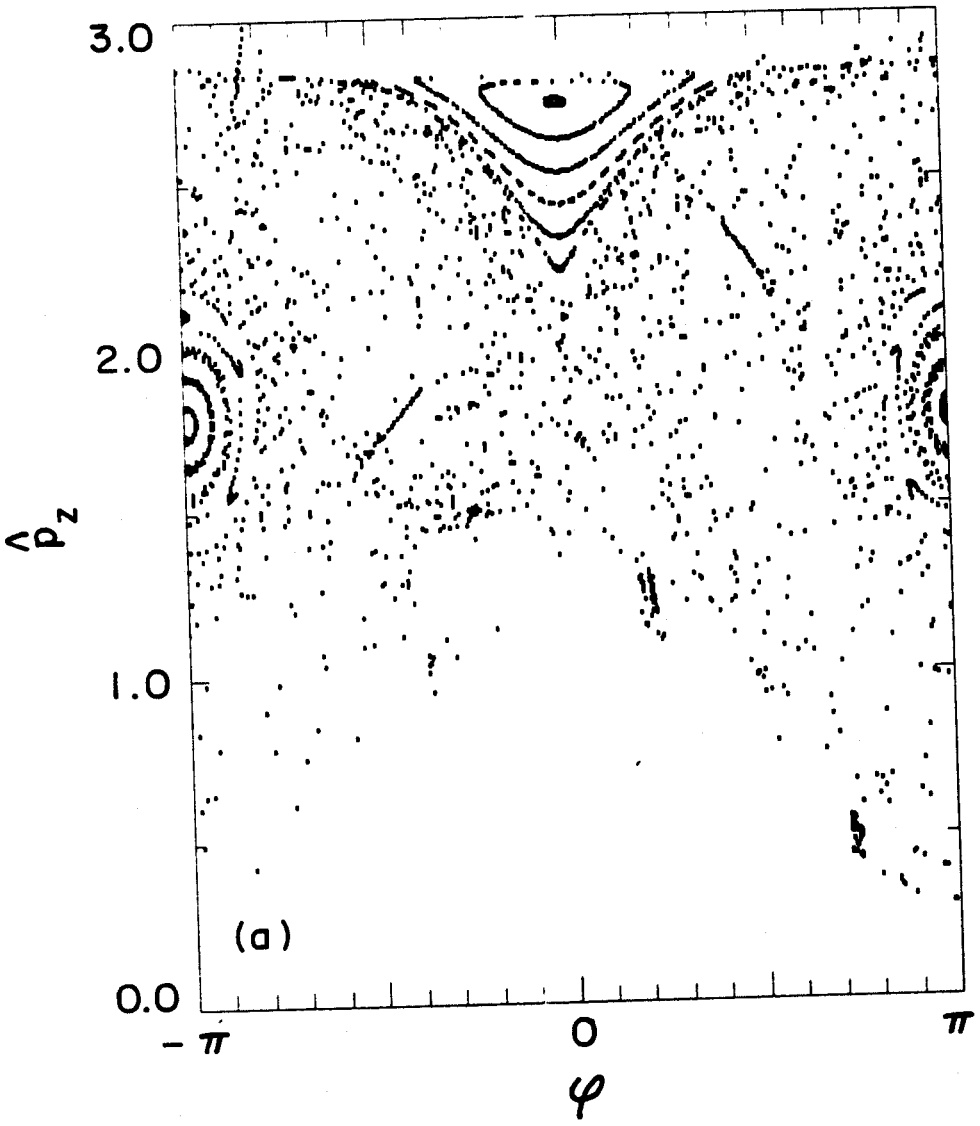

Figure 5a

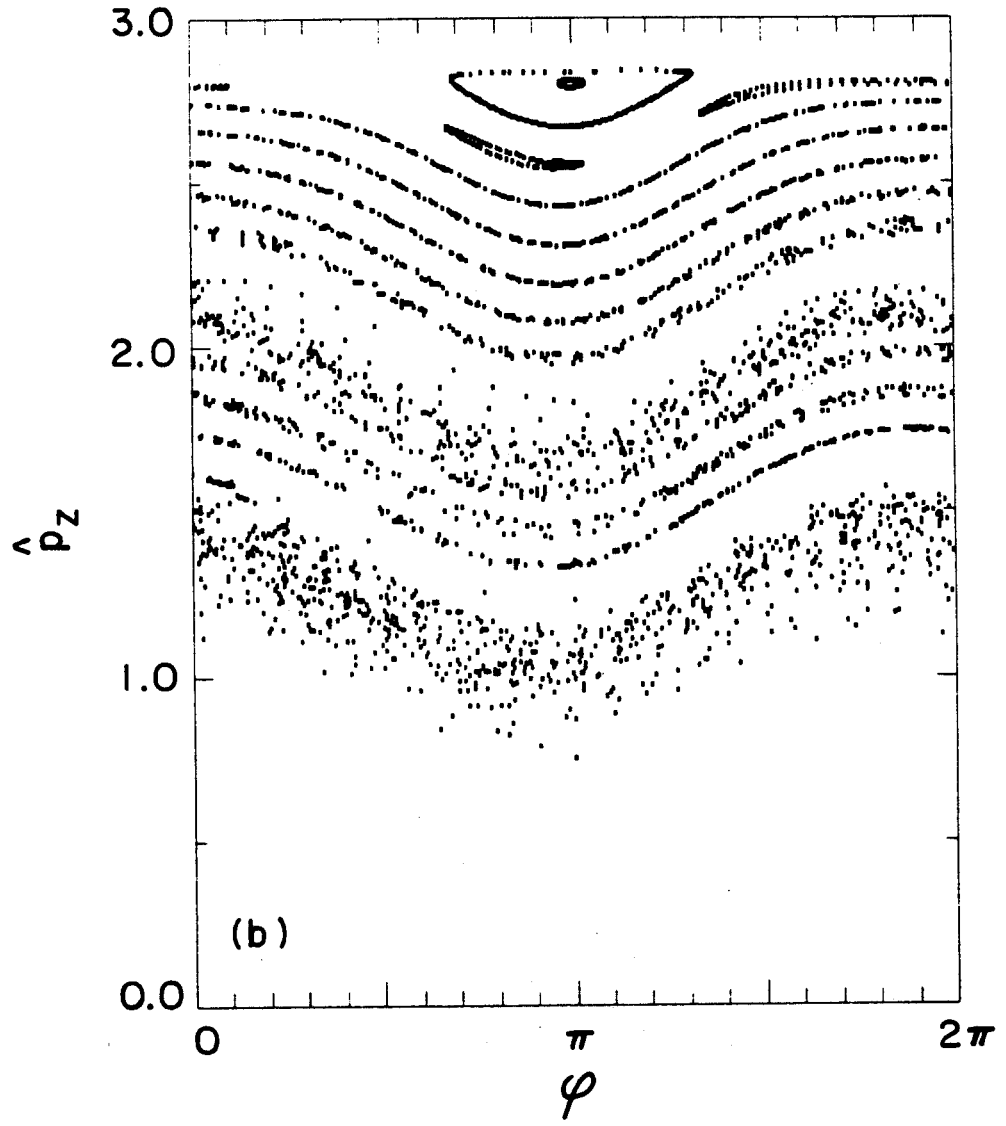

Figure 5b

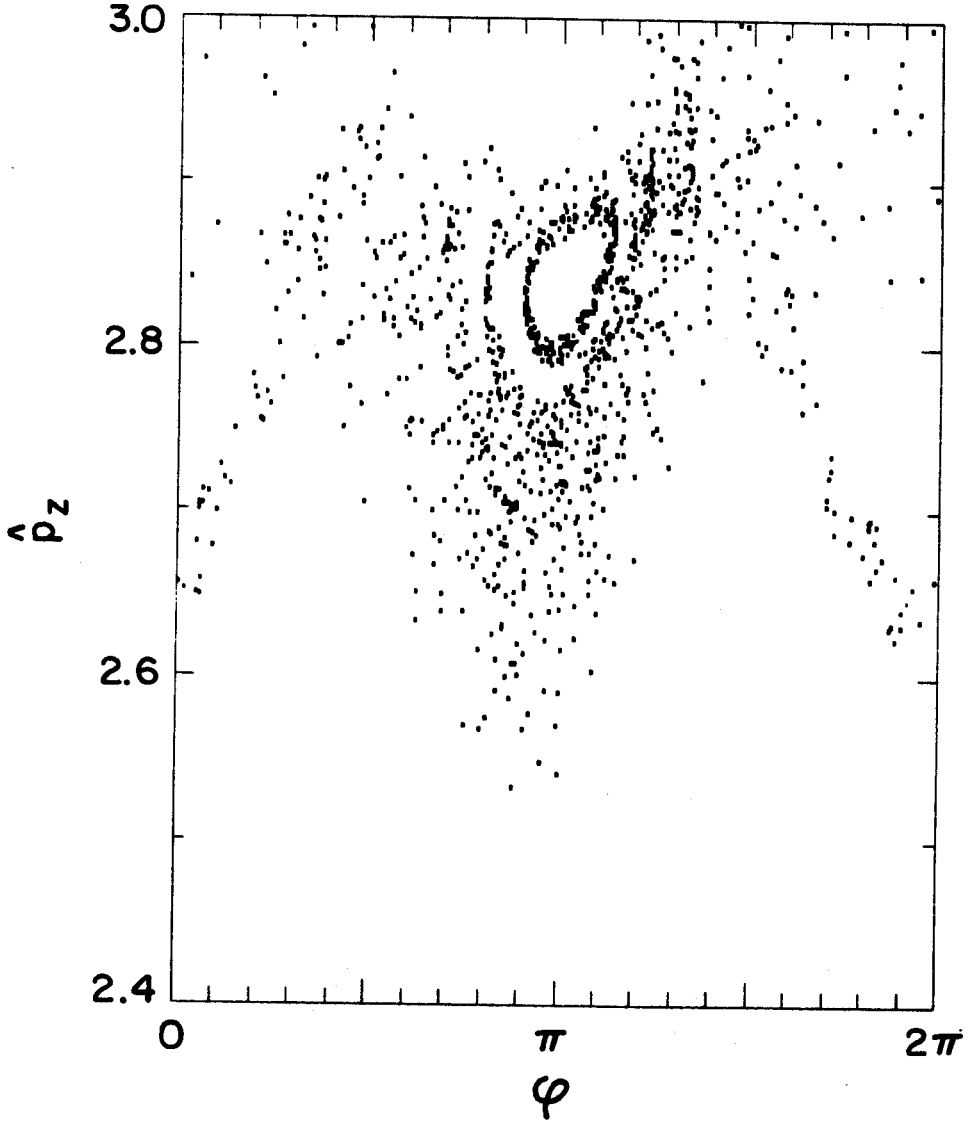

Figure 6